Study on the Analytical Behaviour of Concrete Structure Against Local Impact of Hard Missile

Ahmad Mujahid Ahmad Zaidi [*1], Ismail Abdul Rahman[2], Qadir Bux alias Imran Latif[3]

[1]Department of Mechanical Engineering, Faculty of Engineering
National Defense University Malaysia (UPNM), 57000 Sungai Besi – Kuala Lumpur, Malaysia.
Phone: +60 17 4783139.

[2,3]Faculty of Civil and Environmental Engineering
Universiti Tun Hussein Onn Malaysia, 86400 Parit Raja - Batu Pahat, Johor, Malaysia.

*Corresponding E-mail : mujahid@upnm.edu.my, mujahid80s@yahoo.com

ABSTRACT

Concrete is basic construction material used for almost all kind of structure. However, in the majority essential structures such as nuclear plants, Power plants, Weapon Industries, weapons storage places, water retaining structures like dams, highways barriers, bridges, & etc., concrete structures have to be designed as self-protective structure which can afford any disaster or consciously engendered unpleasant incidents such as incident occurs in nuclear plants, incident in any essential industry, terrorist attack, Natural disasters like tsunami and etc missile attack, and local impact damage generated by kinetic missiles dynamic loading (steel rods, steel pipes, turbine blades, etc.). This paper inquisitively is paying attention on verdict of the recent development in formulating analytical behavior of concrete and reinforced concrete structures against local impact effect generated by hard missile with and without the influence of dimensional analysis based on dominant non-dimensional parameters, various nose shape factors at normal and certain inclined oblique angles. The paper comprises the analytical models and methods for predicting penetration, and perforation of concrete and reinforced concrete. The fallout conquer from this study can be used for making design counsel and design procedures for seminal the dynamic retort of the concrete targets to foil local impact damage.

Keywords: *Concrete, local impact, Hard missile, Analytical models, nose shape, oblique angle, normal, penetration, perforation.*

**Corresponding Author*

1.0 INTRODUCTION

Over the years, concrete is very commonly used construction material for the defensive and civil applications to protect structures from local and explosive impact loads. For the designing of premium shielding structures it is vital to have a good knowledge about deeds of concrete against impact or explosive loading conditions. Projectile may be exists in a long diversity with fluctuation in sizes, shapes, velocity, weight, density, such as bullets, fragments, tornado, terrorist bombing, etc. The projectile may be classified as 'Hard' and 'Soft' depending upon deformability of projectile with respect to target's deformation. Deformation of hard missile is considerable smaller or negligible compared with target's deformation. Almost in all cases hard missiles are considered as non – deformable or rigid. However, 'Soft' missile deforms itself considerably well as compared to target's deformation.

The effects of the local impact of hard missile on structures have been studied since the mid of 17th century because of incessant military attention in designing of high performance missiles and high performance defensive obstructions [2]. A review uncovered that peak studies about concrete structures against dynamic loading were conducted from the early 1940s [57]. However, shortly after World War – II most of the research work ceased and were not resumed until 1960s [57]. Since five decades ago, intensive study on the local impact effects of hard missiles on concrete targets re-initiated by Kennedy in 1976, and provided an early review of the concrete design against missile local impact effects for nuclear industry. Various studies have been conducted to specify the local impact effects of hard missile on concrete structures, which were discussed intensively in previous publications, e.g., [1,2].

The local impact effect of hard missile on concrete structures can be studied by three ways, (i). Empirical Studies (predict empirical formula based on experimental data), (ii). Analytical Studies (create formula based on physical laws and compared with experimental data), and (iii), Numerical Simulation (based on computer based material model generate results and compared with experimental data).

Interest is focused on review of local damage analytical response of concrete and reinforced concrete target deformation caused by 'Hard' missiles considering parametric analysis (velocity of missile, weight of missile, size and shape of missile, angle at which missile struck on target, density of missile and target, thickness of structure, strength of concrete and reinforced concrete, nose shape of missile and etc) with and without the influence of dimensional analysis based on dominant non-dimensional parameters,.

2.0 LOCAL IMPACT

Local impact effect is briefly sub-divided in below explained processes (Fig. 1):

2.1 Radial cracking:

When projectile colloids with concrete target with certain velocity, it results radial cracks originated from the point of impact within the target in every direction [2].

2.2 Spalling:

The ejection of material of target from front face (impacted face) due to impact of hard projectile is called spelling. Spelling produces spall crater in the surrounding area of impact. Spall crater is the total damaged portion of peeling off material from target on impacted face [1, 2].

2.3 Penetration:

Penetration is defined as the digging of missile into the target body afar from the thickness of spall crater. The lengthwise measurement of dig is called penetration depth [1, 2].

2.4 Cone cracking and plugging:

During penetration missile colloids with rear border of target and generates curved shear cracks in the shape of bell plug is called cone cracking. And than missile continues penetrating through target, it forces plug and shears-off the surrounding material of target is called plugging. This process generates rapid change into the behavior of target [2].

2.5 Scabbing:

Ejection of target material from back face of target is called scabbing [1, 2].

2.6 Perforation:

Perforation means complete passage or complete crossing of projectile through the target. It causes missile to extend penetration hole through scabbing crater and exit from the rear face of target [1, 2].

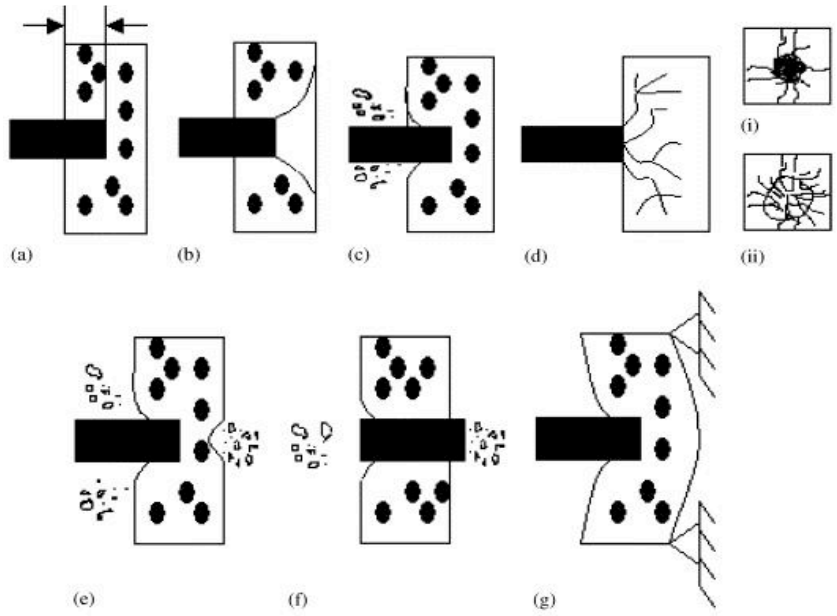

Fig. 1: Explains the local impact phenomena caused by hard projectile. (a) Penetration; (b) cone cracking and plugging; (c) spalling; (d) radial cracking; (e) scabbing; (f) perforation and (g) global impact phenomena [2].

3.0 ANALYTICAL FORMULATION OF PENETRATION DEPTH

3.1 Penetration of Concrete Structures:

The prime issue in an analytical penetration model is to correct formulation of the resultant force (F_R), offered by concrete target on the projectile during penetration process. He suggested the Newton's second law of motion for the linear motion of the rigid projectile:

$$M\frac{dV}{dt} = -F_R\,, \tag{1}$$

With initial conditions $V = V_o$ at $t = 0$, and $X = 0$ at $t = 0$, where $V = (dX/dt)$, X and V are the instantaneous penetration depth and projectile velocity respectively. The above equation controls the motion of projectile and penetration depth.

The penetration resistance formulated as function of the projectile velocity to include the dynamic effects in a penetration process. Often, the penetration resistance force takes the form of binomial function of the instantaneous projectile velocity [4, 5],

$$F_R = F_R(V) = A_1 + A_2V + A_3V^2\,, \tag{2}$$

Where A_1, A_2, and A_3 can be considered as approximate constant parameters determined by the geometry of projectile nose and the mechanical properties of the target. Experimental determination of function F_R (V) in above equation is possible from deceleration-time data in instrumented penetration tests [6]. Forrestal et al. suggested in [6] that a two-term penetration resistance ($A_2 = 0$ in above Eq.) gave excellent agreement with instrumented experimental results, however, it underestimated the experimental results for a 39MPa concrete target when the CRH of the projectile becomes large.

The early work of Robins and Euler in the eighteenth to nineteenth centuries took A1 and A2 equal to zero, which was further developed by Allen et al. [4] to relate the coefficient of the penetration resistance for sand to the drag coefficient as in aerodynamics.

$$F_R = \frac{1}{2}C_d\ell AV^2 \tag{3}$$

Where A, ρ are the presentation area on a plane normal to the flight line, and density of the medium respectively, and C_d is drag co-efficient, for granular medium C_d can be considered as constant over wide velocity range, although for more accuracy it should be formulated as function of the projectile velocity.

Poncelet (1788 – 1867) suggested a more realistic expression for the resistance force function:

$$F_R = A(a + bV^2) \tag{4}$$

Where A is the cross-sectional area of the projectile nose it equals to A0 when the projectile nose is completely embedded into the concrete target, where A0 is the cross-sectional area of the projectile shank), and a and b are constants can be determined by the geometry of the projectile nose and the mechanical properties of target. Poncelet formula further illustrated through dynamic cavity expansion theory. Wen [7, 8] suggested a linear expression of penetration resistance force:

$$F_R = A\left(\alpha f_c + \beta\sqrt{\ell f_c} V\right) \tag{5}$$

Where f_c is quasi-static target material strength, α and β are constants that are determined either experimentally or theoretically. Values of α, β and f_c were recommended for four common nose shapes for various target materials and reasonable agreement between predictions and experimental data were obtained for a collection of penetration and perforation tests [7,8].

Dynamic cavity expansion theory offers a theoretical foundation for the Poncelet resistance function. The pioneer work of Bishop et al. [9] employed quasi-static equations for the expansion of cylindrical and spherical cavities to estimate the resistance force applied on the conical nose when it punches slowly into a metal target. Hill [10] and Hopkins [11] developed the dynamic cavity expansion equations for an incompressible target material, which was applied by Goodier [12], including target inertia effects, to predict the penetration depth of a rigid sphere into metal targets.

In the last decade, the dynamic cavity expansion theory vastly used for the study of deep penetration of projectiles in to metal, concrete and soil targets [13, 14, 15, 16, 17, and 18]. Li and Chen [15] further modified the Forrestal's concrete target penetration model [13, 16] to projectile having general nose shapes and two independent non – dimensional parameters were introduced to determine the penetration depth (x). The axial resistance force on the projectile nose, when the interface friction between the projectile nose and concrete target is neglected:

$$F_R = cx \qquad \text{for } x < kd \tag{6}$$

During spall cratering, and during penetration:

$$F_R = \frac{\pi d^2}{4}\left(Sf_c + N^*\ell V^2\right) \qquad \text{for } x \geq kd \tag{7}$$

Where c can be calculated:

$$c = \frac{\pi d}{4k}\frac{(N^*\ell V_o^2 + Sf_c)}{\left(1 + \left(\frac{\pi k d^3}{4M}\right)N^*\ell\right)} \tag{8}$$

S, k and N can be calculated by using semi analytical formulae given in previous section.

The dynamic cavity expansion theory further modified to accommodate different material characteristics. Xu et al. [20] developed an elastic-cracking resistance force

model based on the dynamic spherical cavity expansion theory when considering the post – test observations that concrete cracks in the region surrounding the projectile. Durban and Masri [21] studied the dynamic cavity expansion theory in pressure – sensitive elastoplastic media based on the Druucker – Prager plasticity model, which has been used as constitutive equation for describing the non – elastic deformation the range of geo – materials and concrete.

In addition the projectile velocity and penetration depth is also considered in the formulation of the penetration resistance function,

$$F_R = F_R(V, x) \tag{9}$$

Murff and Coyle [22] introduced a polynomial function of x and V for penetration into clay:

$$F_R = A_1 + A_2 x + A_3 x^2 + A_4 V + A_5 x V + \ldots\ldots\ldots\ldots, \tag{10}$$

Where co – efficient A_i can be determined from experimental data for variety of projectiles nose length, diameter, and impact velocity,

An approximate penetration theory was established based on impact force time history, which can be represented by Separable force law, that theory engaged in the establishment of the modified NDRC formula [1, 23], viz.

$$F_R = g\left(\frac{x}{d}\right) f(v) \tag{11}$$

Where g – function is non – dimensional and given as:

$$g\left(\frac{x}{d}\right) = \frac{x}{2d} \qquad \text{for } \frac{x}{d} \leq 2.0 \tag{12}$$

$$g\left(\frac{x}{d}\right) = 1 \qquad \text{for } \frac{x}{d} > 2.0 \tag{13}$$

$$f(V) = \frac{1466\sqrt{f_c}}{N^*}\left(\frac{V}{12{,}000d}\right)^{0.2} \qquad \text{(F.P.S)} \tag{14}$$

$$f(V) = \frac{121.7\sqrt{f_c}}{N^*}\left(\frac{V}{1000d}\right)^{0.2} \qquad \text{(S.I)} \tag{15}$$

where n is nose shape factor defined already in modified NDRC formulae, Riera [24] suggested a β – function, for normal penetration distance. The resistance function is independent of V, f(V) = 1, and

$$g\left(\frac{x}{d}\right) = \frac{\pi d^2 f_c \beta}{4}\left(\frac{x}{d}\right) \tag{16}$$

where

$$\beta\left(\frac{x}{d}\right)=\frac{\beta_1-\beta_2\exp\left(-cx/d\right)}{N^*} \tag{17}$$

where N is the nose shape factor introduced in the modified NDRC formulae, the penetration formula was given in terms of the impact factor introduced in [25] and β_1, β_2, c were obtained through regression method by fitting experimental data on penetration depth:

$$I_a=194.59\left(\frac{x}{d}\right)-322.27\left[1-\exp\left(-0.598\frac{x}{d}\right)\right] \tag{18}$$

In early 1970s The AVCO Corporation was proposed an analytical method to provide explicit formulations for the normal and tangential stresses on the projectile based on rigid projectile assumption, by using differential area force law (DAFL)" [26]. They produce this formula in cooperation with six independent linear and momentum equations for rigid body and their respective initial conditions, control the dynamics of a projectile during penetration. Later on the US Army Waterways Experiment Station (WES) modified the DAFL approach to make available 2D (PENCO2D) and 3D (PENCRV3D) codes for projectile trajectory analyses [27 – 29].

In the end, Sandia National Lab has combined dynamic cavity expansion theory with finite element code (PRONTO – 3D) for the study of deformation of projectile and for overall damage [30], where an analytical force function derived from the dynamic cavity expansion theory was used to represent the target and the projectile was simulated by an explicit FE code PRONTO – 3D. This methodology avoids the target discretization, contact algorithms, and verified for metallic and geo – material targets [3, 31 – 33].

Analytical models based on the penetration resistance formulation are efficient, accurate, and capable of predicting the penetration depth into various targets. The dynamics of the projectile motion during penetration can be determined analytically and the nose geometry of the projectile can be included in the model. Since the interactions between the projectile and the target occur on the surface of the projectile, the DAFL method greatly extended the capability of the analytical model into more general simulations of projectile trajectory and deformation.

3.2 Penetration of Reinforced Concrete Structures:

X.W. Chen and X.L. Li suggested an analytical model for penetration depth (x) and for perforation limit (e) of reinforced concrete target. The limitation of that model is projectile impact on concrete target on perpendicular direction, based on dynamic cavity expansion theory normal penetration in concrete target the initial crater is assumed as a cone with axial depth (kd) where k is non-dimensional parameter equals to 0.707 + h/d as given in Li and Chen [15]. For thick concrete targets the axial resistance forces on the projectile nose during the initial cratering and penetration processes:

$$F_R = cx \qquad \text{for x < kd} \tag{19}$$

$$F_R = \frac{\pi d^2}{4}\left(Sf_c + N^* \ell V^2\right) \qquad \text{for x} \geq \text{kd} \tag{20}$$

Where S is an empirical constant related to unconfined compressive strength of concrete f_c, c is experimental constant, x is the instantaneous penetration depth, and ρ is density of concrete target. S can be calculated by [15,16]:

$$S = 72 f_c^{-0.5} \quad \text{or} \quad S = 82.6 f_c^{-0.544} \tag{21}$$

Where f_c is measured in MPa [15, 16], Impact function I, Geometry function N, and Nose function N* are:

$$I = \frac{MV_o^2}{d^3 Sf_c} \tag{22}$$

$$N = \frac{M}{\ell d^3 N^*} \tag{23}$$

$$N^* = -\frac{8}{d^2}\int_0^h \frac{yy'^3}{1+y'^2}dx \tag{24}$$

where y is the geometric definition of the projectile's nose curve. Expressions of N* for various nose shapes can be integrated and have been formulated in Chen and Li [19].Chen et al. [49] formulate that $c = \left(d^2 \pi S f_c / 4k\right)\left((1+I/N)/(1+k\pi/4N)\right)$; when N » I and N » 1, it is further deduced as $c = d^2 \pi S f_c / 4k$. The dimensionless maximum penetration depth for semi-infinite concrete target can be calculated by using:

$$\frac{X}{d} = \sqrt{\frac{(4k/\pi)(1+\pi k/4N)}{(1/I+1/N)}} \qquad \text{for } \frac{x}{d} \leq \text{k} \tag{25}$$

$$\frac{X}{d} = \frac{2}{\pi} N \ln\left[\frac{(1+I/N)}{(1+\pi k/4N)}\right] + k \qquad \text{for } \frac{x}{d} > \text{k} \tag{26}$$

Here the dimensionless penetration depth measured in stages of initial cratering and tunneling is $X/d = \chi\left(1 - H^*/H\right)$. The final penetration depth without perforation can be obtained easily if $I_* = 0$ and considering that no final plugging failure occurs:

$$\chi\left(1 - \frac{H^*}{H}\right) = \sqrt{\frac{(4k/\pi)(1+\pi k/4N)}{(1/I+1/N)}} - \sqrt{\frac{(4k/\pi)(1+\pi k/4N)}{(1/I_*+1/N)}} \qquad \text{for } \frac{x}{d} \leq \text{k} \tag{27}$$

$$\chi\left(1 - \frac{H^*}{H}\right) = \frac{2}{\pi} N \ln\left[\frac{(N+1)}{(1+\pi k/4N)(N+I_*)}\right] + k \qquad \text{for } \frac{x}{d} > \text{k} \tag{28}$$

where $I_* = MV_*^2 / d^3 Sf_c$. For the thick concrete panels, we assume V* to be the velocity of the projectile at the end of penetration, which is determined by the dynamic cavity expansion theory and plug model. For the thin concrete panels, V_* is the velocity

of the projectile at the transitional instant from initial cratering to shear plugging. When N » I, and N » 1, which is associated with sharp and slender projectiles, the final penetration depth can be simplified as:

$$\frac{X}{d} = \sqrt{\frac{4k}{\pi} I} \qquad \text{for } \frac{x}{d} \le \text{k or I} \le \frac{k\pi}{4} \tag{29}$$

$$\frac{X}{d} = \frac{2I}{\pi} + \frac{k}{2} \qquad \text{for } \frac{x}{d} > \text{k or I} > \frac{k\pi}{4} \tag{30}$$

$$X\left(1 - \frac{H^*}{H}\right) = \sqrt{\frac{4k}{\pi} I} \qquad \text{for } \frac{x}{d} \le \text{k or I} \le \frac{k\pi}{4} \tag{31}$$

$$X\left(1 - \frac{H^*}{H}\right) = \frac{2I}{\pi} + \frac{k}{2} \qquad \text{for } \frac{x}{d} > \text{k or I} > \frac{k\pi}{4} \tag{32}$$

3.3 Oblique Penetration of Concrete and Reinforced Concrete Structures:

Consider a model similar to Recht and Ipson [51], and Ipson and Recht [52], with assumption of angular direction (δ) take place near the front surface in the process of initial cratering due to action of asymmetric resistance. Therefore the thickness of target at angle considered as effective thickness of target and it is equal to $H_{eff} = H / \text{Cos}(\beta + \delta)$. According to Forrestal et al. [16, 53], Li and Chen [15, 54] based on dynamic cavity expansion theory there is only drag force along the axial direction of projectile after projectile head entering the concrete target.

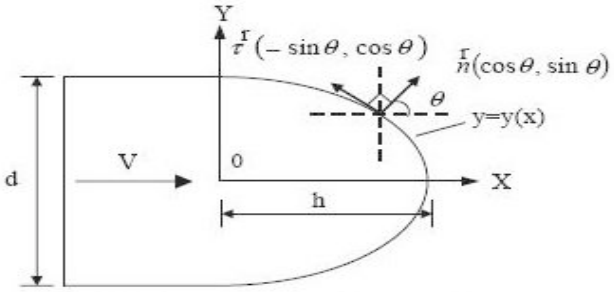

Fig. 2: Explains Cross-section of general nose.

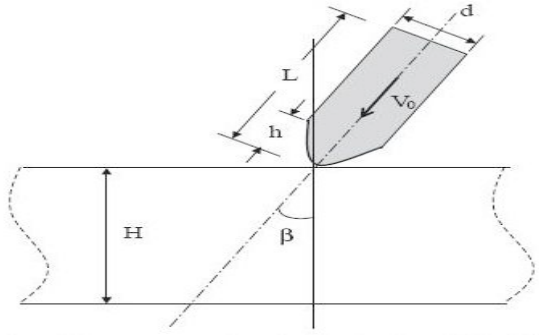

Fig. 3: Explains Penetration and perforation model of concrete target by a rigid projectile at initial obliquity angle β.

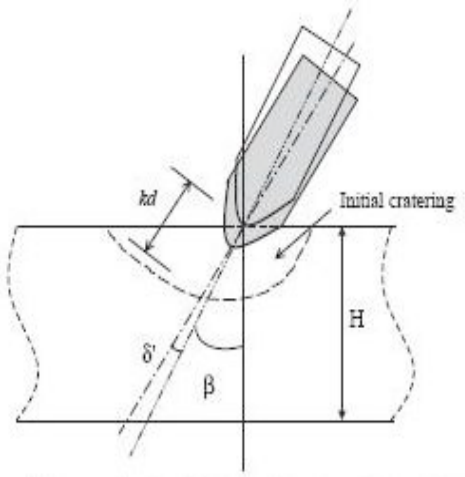

Fig. 4: Explains the first stage of impact Directional change of projectile.

It is known that the impact damage of a concrete target subjected to the normal impact of a rigid projectile consists of a conical crater with depth (kd) and a tunnel with the size of the projectile shank diameter (d), based on slip-line theory Li and Chen [15, 54] suggested k = (0.707 + h/d) for normal impact of hard missile on concrete. Similarly, for oblique penetration, the initial crater is assumed as an oblique-crossed cone with an axial depth kd, where k = (0.707 + h/d)Cosβ.

In [55] experimental results show that the resistant drag increases almost linearly with time in the first stage, so the average lateral force is:

$$F_{\perp avg} = \frac{1}{2} F_o Sin\beta = \frac{1}{2}\frac{cx}{d} Sin\beta \qquad \text{for} \frac{x}{d} \leq k \tag{36}$$

$$F_{\perp avg} = \frac{1}{2} F_o Sin\beta = \frac{1}{2}\frac{d^2\pi}{4}\left(Sf_c + N^* \ell V_o^2\right) Sin\beta \qquad \text{for} \frac{x}{d} > k \tag{37}$$

Where $F_o = c(x/d)$ for $(x/d) \leq k$

$$F_R = \frac{d^2\pi}{4}\left(Sf_c + N^* \ell V^2\right) \qquad \text{for } x \geq kd \tag{38}$$

The kinetic energy consumption normal to submerging path, and the angle of directional changes respectively:

$$\frac{1}{2} M V_\perp^2 = F_{\perp avg} s_\perp \tag{39}$$

$$\sin^2\delta = \delta Sin\beta \left(\frac{1}{V} + \frac{1}{N}\right)\left[\frac{1}{\sqrt{\left(1/ICos^2\delta\right) + \left(1/N\right)}} - \frac{1}{\sqrt{\left(1/I_*\right) + \left(1/N\right)}}\right]^2$$

$$\text{for} \frac{x}{d} \leq k \tag{40}$$

$$Sin^2\delta = \delta Sin\beta \frac{\pi k}{4}\left(\frac{1}{V} + \frac{1}{N}\right) \qquad \text{for} \frac{x}{d} > k \tag{41}$$

By Li and Chen [15, 54] and Chen and Li [19], for sharper nose and slender shrank projectiles in many practical cases N » I, particularly N » 1. As I > I*, for smaller directional change (δ→0):

$$\delta = Sin\beta\left(1-\sqrt{I_*/I}\right)^2 \qquad \text{for}\frac{x}{d}\leq k \qquad (42)$$

$$\delta = \frac{k\pi Sin\beta}{4I} \qquad \text{for}\frac{x}{d}>k \qquad (43)$$

The above equations give the quantitative demonstration on the effects of projectile geometry, target material, impact velocity and initial obliquity on the angle of direction change.

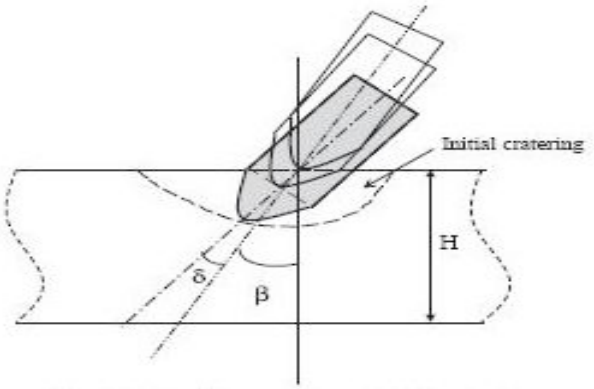

Fig. 5: Explains the end of first stage (Initial cratering).

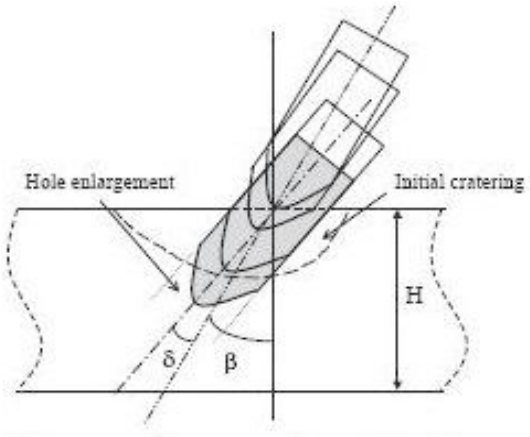

Fig. 6: Explains the tunneling process after dimensional change.

After the initial cratering stage of directional change, the projectile penetrates into target along X direction at an angle of (β + δ) purely followed the dynamic cavity expansion theory. The motion of the rigid projectile is governed by Newton's second law of motion together with initial conditions of $V(t = 0) = V_o\cos\delta$ and $X(t=0) = 0$, can be integrated to obtain the final penetration depth [15, 54]:

$$\frac{X}{d} = \sqrt{\frac{(4k/\pi)(1+k\pi/4N)}{(1/I\cos^2\delta + 1/N)}} \qquad \text{for}\frac{x}{d}\leq k \text{ or } I\cos^2\delta\leq k\pi/4 \qquad (44)$$

$$\frac{X}{d} = \frac{2}{\pi} N \ln \left[\frac{1 + I\cos^2 \delta / N}{1 + k\pi/4N} \right] + k \qquad \text{for} \frac{x}{d} > k \text{ or } I\cos^2\delta > k\pi/4 \tag{45}$$

For N » I and N » 1

$$\frac{X}{d} = \sqrt{\frac{4kI}{\pi} Cos^2 \delta} \qquad \text{for} \frac{x}{d} \leq k \text{ or } I\cos^2\delta \leq k\pi/4 \tag{46}$$

$$\frac{X}{d} = \frac{2I\cos^2 \delta}{\pi} + \frac{k}{2} \qquad \text{for} \frac{x}{d} > k \text{ or } I\cos^2\delta > k\pi/4 \tag{47}$$

The above equation can be used to predict the penetration depth of hard missile into the thick concrete structures at oblique impact.

4.0 ANALYTICAL FORMULATION OF PERFORATION LIMIT

4.1 Perforation of Concrete Structures

Corbett et al. [34] introduced a multi – stage models, firstly applied for metallic targets. Later on yankelevsky [35] proposed Two – stage model for perforation of concrete targets against the impact of hard missile under low velocities. The first stage is dynamic penetration, where a disk model developed to calculate the stress field and the penetration resistance in front of the projectile nose. The second stage is plug formation and the shear – out of the plug. And during transition phase from first stage to second stage, the total penetration resistance in front of the projectile nose equals to shear resisting force offered by the remaining thickness of the target [36].

$$F_R = \tau_f A_s Cos(\alpha) \tag{48}$$

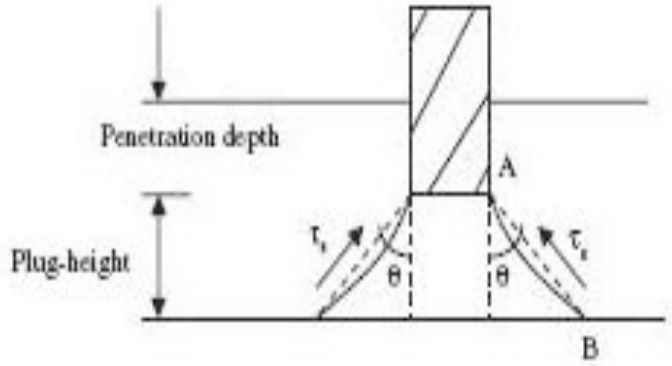

Fig. 7: Explains the multi-stage perforation model for concrete targets.

Where α is cone slope angle, and A_s is the surface area of cone plug. The two stage mechanism agrees with experimental observations that there are clear distinctions between the penetration and plugging processes. Li and Tong [36] combined the shear plug model with the penetration model for cratering and penetration to formulate the perforation of the concrete target. The normalized perforation limit (e) can be determined by:

$$\frac{e}{d}=\frac{H}{d}+\frac{x}{d} \tag{49}$$

Where non-dimensional plug thickness H/d is:

$$\frac{H}{d}=\frac{1}{2\tan(\alpha)}\left[\sqrt{1+2S\tan(\alpha)\left[\frac{3I(1+(I/N))}{\pi k(1+(\pi k/4N))}\right]^{1/2}}-1\right] \quad \text{for } \frac{x}{d}\le k \tag{50}$$

$$\frac{H}{d}=\frac{1}{2\tan(\alpha)}\left[\sqrt{1+\sqrt{3}S\tan(\alpha)}-1\right] \qquad \text{for } \frac{x}{d}>k \tag{51}$$

The non-dimensional perforation ballistic perforations limit (e):

$$\frac{V_{BL}}{\sqrt{f_{cn}d^3/M}} \tag{52}$$

Where f_{cn} is the nominal strength of concrete target (f_{cn} = 40MPa as the unconfined compressive strength of a normal strength of concrete), is determined by:

$$\frac{V_{BL}}{\sqrt{f_{cn}d^3/M}}=\sqrt{\frac{\pi kS}{3}}\sqrt{\frac{f_c}{f_{cn}}}\left[\frac{1}{2S\tan(\alpha)}(Y-1)\right]$$

For $$\frac{V_{BL}}{\sqrt{f_{cn}d^3/M}}\le\sqrt{\frac{\pi kS}{3}}\sqrt{\frac{f_c}{f_{cn}}} \tag{53}$$

$$\frac{V_{BL}}{\sqrt{f_{cn}d^3/M}}=\sqrt{S}\sqrt{\frac{f_c}{f_{cn}}}\left[\frac{\pi}{2}\left(\frac{H_o}{d}-\frac{k}{2}-\frac{\sqrt{\sqrt{3}S\tan(\alpha)+1}-1}{2\tan(\alpha)}\right)\right]^{1/2}$$

For $$\frac{V_{BL}}{\sqrt{f_{cn}d^3/M}}\ge\sqrt{\frac{\pi kS}{3}}\sqrt{\frac{f_c}{f_{cn}}} \tag{54}$$

where

$$Y=\frac{3S^2}{16k^2}\left[\sqrt{1+\frac{8k}{\sqrt{3}S}\left(1+\frac{2k}{\sqrt{3}S}+2\left(\frac{H_o}{d}\right)\tan(\alpha)\right)}-1\right]^2 \tag{55}$$

Here N » 1 are assumed, N and I are geometry and impact functions respectively. These conditions can be expressed explicitly by V_o « $(S_f/\rho)^{1/2}$ and $(M/\rho d^3)$ » 1. It should be noted that the expression of Y in [36] is incorrect, [2]. In calculations, a representative value of $\alpha = 70^o$ based on Dancygier's [37] experimental results for normal and high strength concrete is used. It was found that the perforation limit (e) is insensitive to the cone slope angle. This model was verified using test data from [38,39]. A two-stage

model was also recommended by the UKAEA [40] for through-thickness cone cracking. The impact velocity to initiate through-thickness cone cracking, V_{cc}, may be estimated by the following equations:

$$V_{cc} = 9.4 \cdot 10^{-2} \sqrt{f_c} \left(\frac{dH_o^2}{M} + \frac{H_o^3}{M} \right)^{\frac{1}{2}} \quad \text{for } 0.5 < \frac{H_o}{d} \leq 1.82 \tag{56}$$

$$V_{cc} = 0.117 \sqrt{f_c} \left(\frac{H_o^3}{M} \right)^{\frac{1}{2}} \quad \text{for } 1.82 < \frac{H_o}{d} < 4.0 \tag{57}$$

Which were validated for $26<f_c<35$(MPa), $24{,}000<M/(d^2H_o)<1.5\text{x}106$(kg/m^3) and $2<V_{cc}<4.5$(m/s). In the range $1.82<H_o/d<4$, penetration and then a cone crack were produced at the cone cracking velocity, (V_{cc}). For $0.5<H_o/d\leq1.82$, cone cracking occurred from the beginning and was not preceded by penetration. Multi-stage models have not considered possible scabbing on the distal surface of the target. Experimental results and empirical formulae support the contention that the scabbing limit is generally greater than the perforation limit, i.e. $h_s>e$. This indicates three possibilities: (a) if $H_o>h_s$, both scabbing and perforation do not occur, (b) if $h_s>H_o>e$, scabbing occurs without perforation and (c) if $h_s>e>H_o$, both scabbing and perforation occur. Because scabbing removes material from the distal side of the target, it could play an important role in the initiations of both perforation and cone cracking. This issue should be further investigated.

4.2 Perforation of Reinforced Concrete Structures

The model for perforation limit of reinforced concrete target against hard missile suggested by X.W. Chen and X.L. Li based on shear plugging criteria. The formation of plug is related with shear failure of target, at normal impact plug considered as cone shape with the cone slope angle (α), $\alpha = 60^o$ [35, 37, and 50] for normal plain concrete, however because of reinforcement, in reinforced concrete the residual height of cone shaped plug may become thinner and cone slope angle (α) may become increase also. In this model X.W. Chen and X.L. Li assumed a general cone slope angle (α) for formulation, A_s is the shear surface area of the cone shaped plug, and H* is cone-shaped plug or residual thickness of the rear crater. In the case of normal perforation, the shear area of the conical plug surface is:

$$A_s = \frac{\chi \pi d^2 H^*}{H Cos\alpha} \left(1 + \chi \frac{H^*}{H} \tan\alpha \right) \tag{58}$$

In plain concrete it is assumed that the plug is separated from surrounding of concrete as soon as the shear failure criteria satisfied along the plug surface. The failure stress in pure shear (ζ_f) is equal to ($3^{-0.5}$fc). In reinforced concrete target the tensile failure of reinforcement should be considered during the separation of rear plug from the target.

In reinforced concrete targets may be some other case exists rear crater may be occurs in concrete without reaching tensile yield in reinforced bars. In this case projectile may be unable to perforate the reinforced concrete target resisted by reinforcement. Thus the failure criteria defined in two phases: Shear failure of concrete and tensile failure of reinforced bars, and shear plugging occurs as soon as the resistant force ahead of the projectile nose reaches a critical value:

$$F = \frac{1}{\sqrt{3}} f_c A_s Cos\alpha + 2\pi R_d H \ell_s f_s Sin\alpha \tag{59}$$

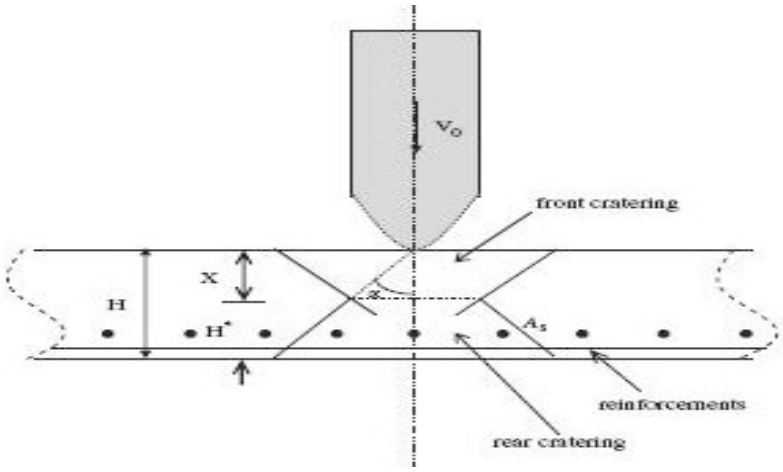

Fig. 8: Explains the Normal perforation of thin reinforced concrete targets (no tunneling process).

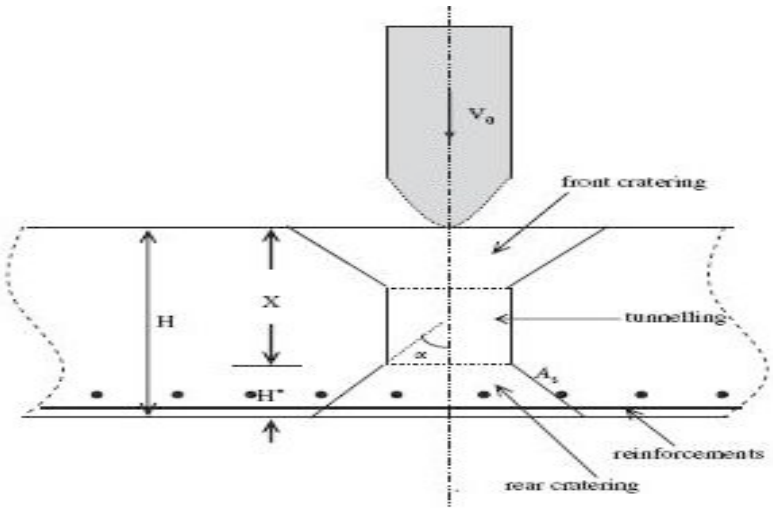

Fig. 9: Explains the Normal perforation of thick reinforced concrete targets.

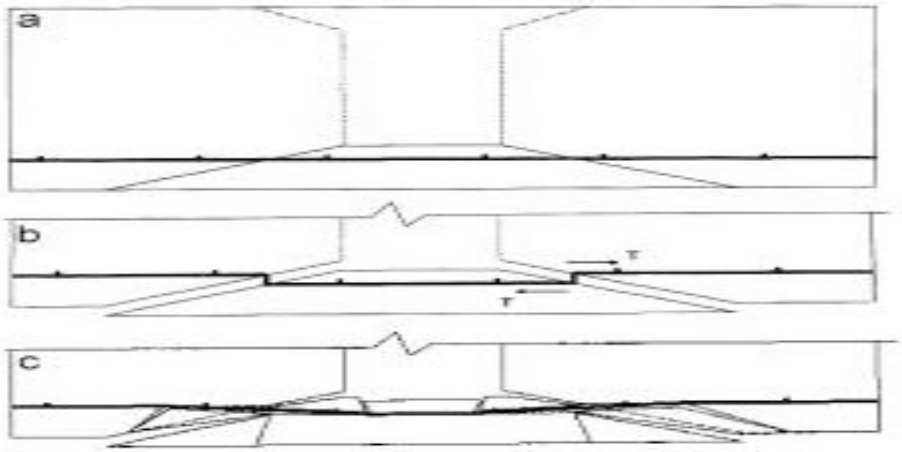

Fig. 10: Explains the schematic description of the failure process at rear face of reinforced concrete targets (after Dancygier [56]).

Here the right hand side of above equation is equal to force component in the motion direction derived from the total shear plug surface, and the Sin(α) in second term gives assumption about the reinforcement bar is normal to the conical plug surface after rotating an angle at the moment of plugging failure. R_d is the radius of cross-section or rear plug in which the layout of reinforcement bars is located, it is assumed to be the middle cross section of the plug, R_d can be calculated by:

$$R_d = \frac{d}{2} + \frac{H^*}{2}\tan\alpha \tag{60}$$

Besides considering the three dominant dimensionless numbers in the perforation of concrete slabs, i.e., the impact function I, the geometry function of projectile N and the dimensionless thickness of concrete panel x, reinforcement ratio ρ_s of concrete and the uni-axial tensile strength f_s of reinforcing steel bars are considered as the other main factors influencing the perforation process. In general, f_s represent material property of reinforcing bars, and ρ_s generally depicts the geometric character of reinforcing meshes, which includes the mesh size, space and diameter of reinforcing bars, etc. Therein a dimensionless number is introduced, which is simultaneously related to the reinforcement ratio ρ_s and the uni-axial tensile strength f_s of reinforcing bars.

$$\Theta = \sqrt{3}\chi\ell_s\frac{f_s}{f_c}Sin\alpha \tag{61}$$

$$\frac{H^*_{BL}}{d} = \frac{\sqrt{\left(1+\sqrt{3}S/4k+\Theta\tan\alpha\right)^2+\left(\sqrt{3}S\chi/k-4\Theta\right)\tan\alpha}-\left(1+\sqrt{3}S/4k+\Theta\tan\alpha\right)}{2\tan\alpha}$$

$$\text{for } \frac{x}{d} \le k \tag{62}$$

$$F = \frac{1}{\sqrt{3}}f_c A_s Cos\alpha\left(1+\Theta\frac{d}{H^*}\right) \tag{63}$$

In which Θ = 0 represents the case of plain concrete.

$$A_s Cos\alpha\left(1+\Theta\frac{d}{H^*}\right) = \frac{\sqrt{3}\pi d^2 S\chi}{4k}\left(1-\frac{H^*}{H}\right) \quad \text{for } \frac{x}{d} \le k \tag{64}$$

$$A_s Cos\alpha\left(1+\Theta\frac{d}{H^*}\right) = \frac{\sqrt{3}\pi d^2 S}{4k} \quad \text{for } \frac{x}{d} > k \tag{65}$$

Obviously, A_s and H*/H are independent of initial impact velocity V_o and can be determined by the geometric configuration of perforation. It is only induced from the assumption of N » I and N » 1 and a more general conclusion cannot be achieved.

In fact, the plug always disintegrates into fragments due to the low tensile strength of concrete, which is about one-tenth of the compressive strength. The disintegration is caused by the tensile stresses arising from the reflections of the stress wave prior to shear plugging. Herein we regard V_* as the residual/exit velocity V_r of the projectile after perforation. The ballistic limit is obtained when $V_* = I_* = 0$. We assume that the ballistic limit is V_{BL} and corresponding impact function is $I_{BL} = (MV_{BL}^2)/d^3Sf_c$. For normal

perforation with N » I and N » 1, which are the most common cases in practice, with reference to Chen et al. [49], simplified formulae for ballistic performance of the perforation of reinforced concrete targets is as follows:

$$I_{BL} = \frac{\pi}{4k}\left(\frac{X}{d}\right)^2 = \frac{\pi}{4k}\left(\chi - \frac{H^*_{BL}}{d}\right)^2 \qquad \text{for } \frac{x}{d} \le \text{k} \tag{66}$$

$$I_{BL} = \frac{\pi}{2}\left[\chi\left(1 - \frac{H^*_{BL}}{H}\right) - \frac{k}{2}\right] \qquad \text{for } \frac{x}{d} > \text{k} \tag{67}$$

where the thickness of conical plug $H_{BL}{}^2$ is determined by the following equations:

$$\frac{H^*_{BL}}{d} = \frac{\sqrt{(1+\Theta\tan\alpha)^2 + \left(\sqrt{3}S - 4\Theta\right)\tan\alpha} - (1+\Theta\tan\alpha)}{2\tan\alpha} \qquad \text{for } \frac{x}{d} > \text{k} \tag{68}$$

$$\frac{H^*_{BL}}{d} = \frac{\sqrt{(1+\Theta\tan\alpha)^2 + \left(\sqrt{3}S(X/kd) - 4\Theta\right)\tan\alpha} - (1+\Theta\tan\alpha)}{2\tan\alpha} \qquad \text{for } \frac{x}{d} \le \text{k} \tag{69}$$

On the other hand, the thickness of concrete target should equal the sum of the thickness of the rear plug and the penetration depth measured in the stages of initial cratering and tunneling, i.e.,

$$\chi = \frac{X}{d} + \frac{H^*}{d} \tag{70}$$

Therein the dimensionless critical thickness of concrete target, at which the tunneling process can be either considered or omitted, is introduced as follows:

$$\chi_c = \frac{H_c}{d} = \frac{\sqrt{(1+\Theta\tan\alpha)^2 + \left(\sqrt{3}S - 4\Theta\right)\tan\alpha} - (1+\Theta\tan\alpha)}{2\tan\alpha} + k \tag{71}$$

It is achieved at X/d = k. Since the conical slope angle a and the empirical constant S are mainly determined by the strength of concrete target [15, 19, 35–37, 50], it evident χ_c, which is dominated by the strength of concrete target and the dimensionless number Θ of reinforcing bars. Essentially, the critical conditions X/d ≤ k (or $I_{BL} \le k\pi/4$) and X/d > k (or $I_{BL} > k\pi/4$) correspond to $\chi \le \chi_c$ and $\chi > \chi_c$, respectively. χ_c is introduced to classify the critical thin panels from the general reinforced concrete targets, at which only the front and rear craters are taken into account for the perforation, while the tunneling process is not involved. Therein the ballistic limit can be further formulated:

$$V_{BL} = \sqrt{\frac{\pi d^3 S f_c}{4kM}}\left(\chi - \frac{H^*_{BL}}{d}\right) \qquad \text{for } \chi \le \chi_c \tag{72}$$

$$V_{BL} = \sqrt{\frac{\pi d^3 S f_c}{2M}}\left(\chi - \chi_c + \frac{k}{2}\right) \qquad \text{for } \chi > \chi_c \tag{73}$$

Obviously, the performance of reinforced concrete target (thickness and strength as well as the reinforcing bars) and the geometry of projectile (mass and diameter) dominate the ballistic limit VBL. In the case of $\chi \leq \chi_c$, the ballistic limit VBL is a weakly linear function of dimensionless thickness χ of reinforced concrete target, whilst the variation of VBL with χ is parabolic when $\chi > \chi_c$. If the impact velocity Vo > VBL, the residual velocity of projectile after perforation can be formulated as [49]:

$$V_* = (V_o - V_{BL}) \qquad \text{for } \chi \leq \chi_c \tag{74}$$

$$V_* = \sqrt{(V_o^2 - V_{BL}^2)} \qquad \text{for } \chi > \chi_c \tag{75}$$

The above equations directly suggest conservation of momentum and energy, respectively, which results from the assumption of N » I and N » 1 as well as the different resistance forces. It is worth mentioning that the theoretical curves of residual velocity vs impact velocity are quite different for concrete targets of different thickness. If the target is thick enough, i.e., tunneling needs to be considered, the curve is hyperbolic. Otherwise, it is a straight line if the target is so thin that no tunneling occurs.

Therefore, the perforation limit (e) without the occurrence of plugging can be determined by:

$$\frac{e}{d} = \frac{X}{d} + \frac{H_{BL}^*}{d} \tag{76}$$

$$\frac{e}{d} = \frac{X}{d} + \frac{\sqrt{(1+\Theta\tan\alpha)^2 + \left(\sqrt{3}S(X/kd) - 4\Theta\right)\tan\alpha} - (1+\Theta\tan\alpha)}{2\tan\alpha}$$

$$\text{for } \frac{x}{d} \leq k \tag{77}$$

$$\frac{e}{d} = \frac{X}{d} = \frac{\sqrt{(1+\Theta\tan\alpha)^2 + \left(\sqrt{3}S - 4\Theta\right)\tan\alpha} - (1+\Theta\tan\alpha)}{2\tan\alpha}$$

$$\text{for } \frac{x}{d} > k \tag{78}$$

It is worthwhile to mention that, if $\Theta = 0$, all the above formulations are reduced to the scenario of normal perforation of plain concrete slabs by rigid projectiles, and much simpler solutions of ballistic performance and perforation limit than Li and Tong [36] and Chen et al. [49], are:

$$\frac{e}{d} = \frac{X}{d} + \frac{\sqrt{1 + \left(\sqrt{3}S(X/kd)\right)\tan\alpha} - 1}{2\tan\alpha} \qquad \text{for } \frac{x}{d} \leq k \tag{79}$$

$$\frac{e}{d} = \frac{X}{d} = \frac{\sqrt{1 + \left(\sqrt{3}S\right)\tan\alpha} - 1}{2\tan\alpha} \qquad \text{for } \frac{x}{d} > k \tag{80}$$

4.3 Oblique Perforation of Concrete and Reinforced Concrete Structures

For oblique impact as similar to normal impact only with the change of plug is idealized as an oblique crossed cone having same cone slope angle as in normal impact α with the oblique crossed angle (β + δ).

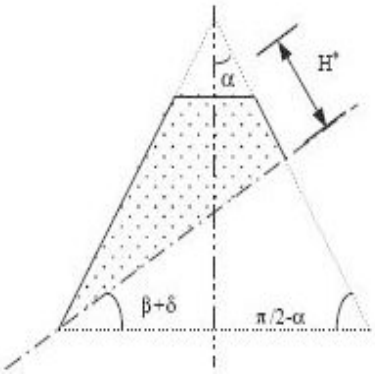

Fig. 11: Explains the geometric sketch of rear, oblique crossed cone crater.

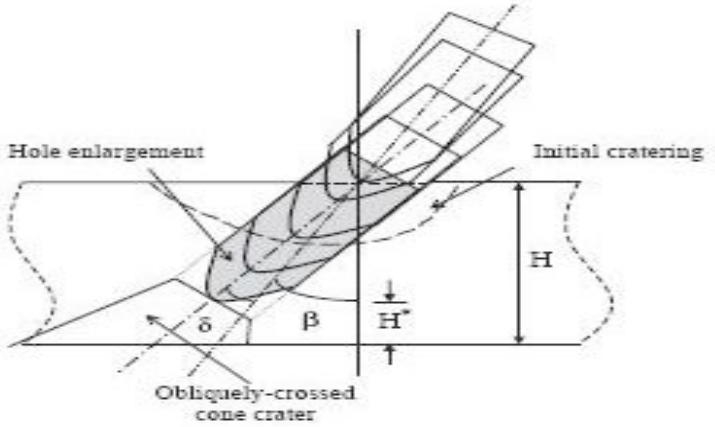

Fig. 12: Explains initiation of rear cratering.

The failure stress in pure shear $\zeta_f = 3^{-0.5}$fc, as concrete is brittle material having low tensile strength approximately equal to 10% of the compressive strength, because of this reason plug is separated from the surrounding material as soon as shear failure criterion satisfied along the plug surface. The disintegration is caused by the tensile stresses arising from the complicated reflections of stress wave prior to shear plugging. It is assumed that A_s is the shear surface area of the oblique crossed cone plug, and H* is the residual thickness of the oblique crossed cone plug, i.e., the normal distance between the rear face and the nose tip. A_s and H* are the functions of α, β, and δ, which can be determined by simple geometrical relations.

There're two scenarios for perforation:

- Initial cratering immediately followed by shear plugging ($x/d \leq k$), no hole enlargement, and

- Complete perforation ($x/d > k$), in which penetration process is also included.

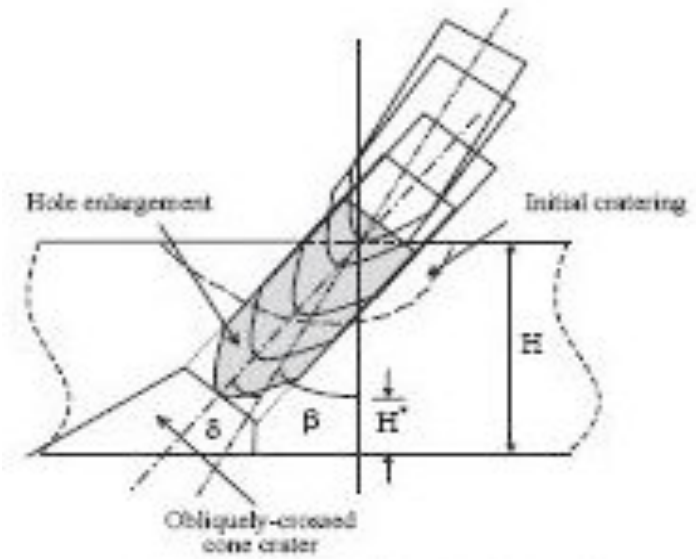

Fig. 13: Explains the Initiation of rear cratering (with tunneling process).

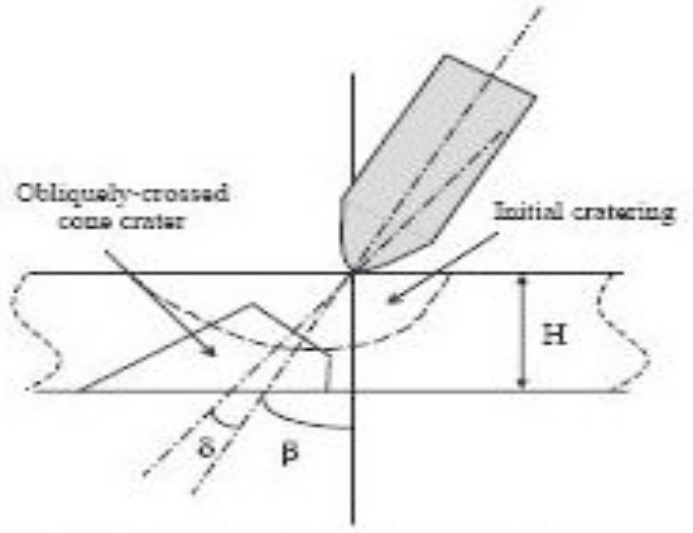

Fig. 14: Explains the oblique perforation of thin concrete target (no tunneling process).

The dimensionless penetration depth measured along the oblique angle (β + δ) in the stages of initial cratering and tunneling in x/d = (H – H*) Sec(β + δ) / d. For different scenarios of perforation, it can be formulated:

$$\chi \sec(\beta+\delta)\left(1-\frac{H^*}{H}\right)=\sqrt{\frac{(4k/\pi)(1+k\pi/4N)}{\left[(1/(I\cos^2\delta))+(1/N)\right]}}-\sqrt{\frac{(4k/\pi)(1+(k\pi/4N))}{\left[(1/I_*)+(1/N)\right]}}$$

$$\text{for}\frac{x}{d}\leq k \qquad (81)$$

$$\chi \sec(\beta+\delta)\left(1-\frac{H^*}{H}\right)=\frac{2}{\pi}N\ln\left[\frac{(N+I\cos^2\delta)}{(1+k\pi/4N)(N+I_*)}\right]+k$$

$$\text{for}\frac{x}{d}>k \qquad (82)$$

Where $\chi = H/d$ is the dimensionless thickness of concrete target. Since concrete is brittle material, shear plugging occurs as soon as the resistance force ahead of the projectile nose reaches a critical value:

$$F = \frac{1}{\sqrt{3}} f_c A_s Cos\alpha \tag{83}$$

Where right hand side of above equation is the force component in the motion direction derived from the total shear plug surface,

$$\frac{f_c A_s Cos(\beta+\delta)}{\sqrt{3}c\chi} = \left(1 - \frac{H^*}{H}\right) \qquad \text{for} \frac{x}{d} \le \text{k} \tag{84}$$

$$\frac{1}{\sqrt{3}} f_c A_s Cos\alpha = \frac{\pi d^2}{4}\left(Sf_c + N^* \ell V_*^2\right) \qquad \text{for} \frac{x}{d} > \text{k} \tag{85}$$

$$\left(1 + \frac{k\pi}{4N}\right)\exp\left[\frac{\pi\chi Sec(\beta+\delta)}{2N}\left(1 - \frac{H^*}{H}\right) - \frac{k\pi}{2N}\right] = \frac{\sqrt{3}S\pi d^2}{4A_s \cos\alpha}\left(1 + \frac{I\cos^2\delta}{N}\right)$$

According to the definitions of c, δ, and A_s, above equations manifest the dependence of H*/H on the initial velocity V_o and the geometric configuration in both cases ($x/d \le k$ and $x/d > k$). If N » I and N » 1 then:

$$A_s \cos\alpha = \frac{\sqrt{3}\pi d^2 S\chi}{4kCos(\beta+\delta)}\left(1 - \frac{H^*}{H}\right) \qquad \text{for} \frac{x}{d} \le \text{k} \tag{86}$$

$$A_s \cos\alpha = \frac{\sqrt{3}\pi d^2 S}{4} \qquad \text{for} \frac{x}{d} > \text{k} \tag{87}$$

Furthermore, if I is large enough (I > 10 or V_o > 500m/s), the angular directional change δ is negligible regardless of the target thickness. Besides, A_s and H*/H are independent of initial impact velocity V_o and can be determined by the geometric configuration of perforation.

In Case of N » 1

To achieve perforation, a projectile having slender shank and sharp nose (e.g., ogive or conical shapes) is frequently used. It corresponds to a larger value of the geometry function N(~200) [54, 55]. For the cases of N » 1, which are the common cases in practice, much simpler formulae can be deduced. The ballistic limit can be simplified as:

$$I_{BL} = \left[\frac{A_{sBL} Cos\alpha Sec\delta_{BL}}{d^2 S}\sqrt{\frac{4k}{3\pi}}\right]^2 \qquad \text{for} \frac{x}{d} \le \text{k (It implies } I_{BL} \ll \text{N)} \tag{88}$$

$$I_{BL} = \frac{\pi Sec^2\delta_{BL}}{2}\left[\chi \sec(\beta+\delta_{BL})\left(1 - \frac{H^*_{BL}}{H}\right) - \frac{k}{2}\right] \qquad \text{for} \frac{x}{d} > \text{k} \tag{89}$$

$$I_* = \left[\sqrt{\frac{I\cos^2\delta}{\left(1+\left(I\cos^2\delta/N\right)\right)}} - \sqrt{\frac{I_1\cos^2\delta}{1+\left(I/N\right)}}\right]^2 \qquad \text{for}\frac{x}{d}>\text{k} \tag{90}$$

$$I_* = \left(I - I_1\right)Cos^2\delta \qquad \text{for}\frac{x}{d}\leq\text{k} \tag{91}$$

It should be noted that I_1 has the same expression as IBL except that δ_{BL} is replaced by a different value of angular directional change δ, which is determined mainly by I. Particularly, if the velocity of projectile is less than 500 m/s, its impact function I is usually less than or around 10, and in this case, eq. (91) can be simplified as:

$$I_* = \left[\sqrt{I} - \sqrt{I_1}\right]^2\cos^2\delta \qquad \text{for}\frac{x}{d}\leq\text{k} \tag{92}$$

On the other hand, if a projectile impacts a concrete target at higher velocities (say 500m/sec < V_o < 1000m/sec), I_* can be expressed only in terms of I and N, and the angle of directional change δ vanishes.

$$I_* = \frac{\left(\sqrt{I} - \sqrt{I_1}\right)^2}{1+I/N} \qquad \text{for}\frac{x}{d}\leq\text{k} \tag{93}$$

$$I_* = \left(I - I_1\right) \qquad \text{for}\frac{x}{d}>\text{k} \tag{94}$$

5.0 CONE CRACKING

The concrete have much lower tensile strength than the compressive strength of concrete, in most cases tensile strength of concrete is equal to 10% of its compressive strength. The cone slope angle is defined as the angle between the direction of motion of the projectile and the side of the cone as an idealization of the ejected plug. The determination of Cone cracking angle of a concrete target subjected to hard missile impact is necessary to estimate the level of damage, although it cause only a small variation in the estimation of perforation limit but from analytical model point of view it should be considered [36]. The separation of cone plug or cone cracking is depends on the local tensile strength and the maximum tensile strength of concrete target. Mostly two extreme cases are considered as reason for the cone cracking angle and the average shear resistance stress on the cone plug.

Case (a) is associated with the stress states along the perimeter of the projectile on the proximal side, and

Case (b) is associated with the stress states along the distal side of the impact.

Case (a): $\sigma_z = -f_c$, $\sigma_r = -f_c$, and $\zeta_{zr} \neq 0$ ($\sigma_z = \sigma_r$, and $\zeta_{zr} \neq 0$):

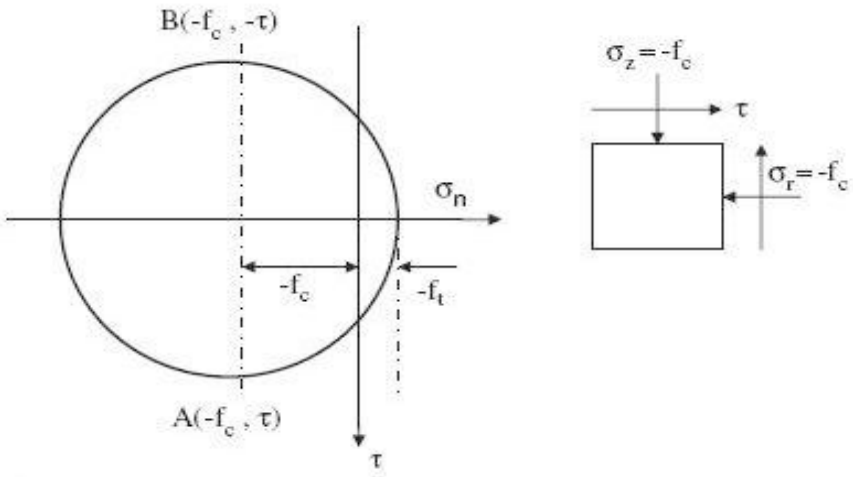

Fig. 15: Explains the Mohr's circle different stress states for case (a).

According to Mohr's circle stress state:

$$\tau = f_c + f_t \approx 1.1 f_c \tag{95}$$

When the maximum tensile stress equals the maximum tensile strength of the concrete, the tensile strength of concrete is assumed to be 10% of the unconfined compressive strength. Under this stress state condition, the maximum tensile failure occurs at the angle of:

$\alpha = 45o$,

This angle is considered as the starting angle of cone cracking, and it is verified with the experimental observations in BNFL [42].

Case (b): $\sigma_z = -f_c$, $\sigma_r = 0$, and $\zeta_{zr} \neq 0$: According to Mohr's circle stress state for this case:

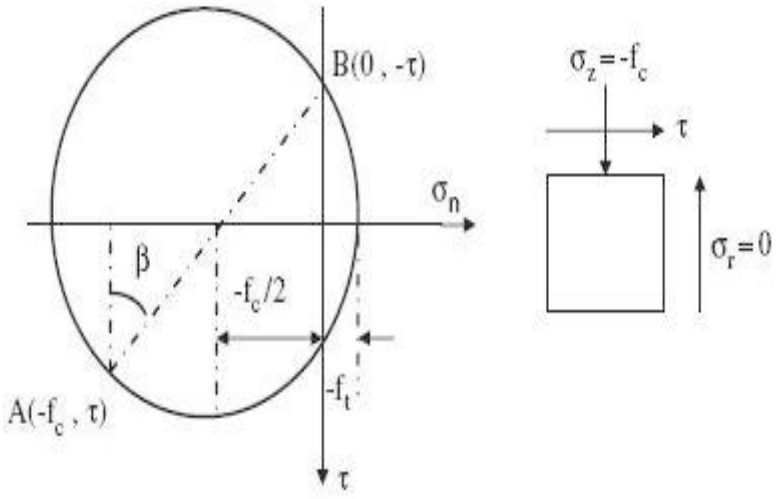

Fig. 16: Explains the Mohr's circle different stress states for case (b).

When the maximum tensile stress equals to the maximum tensile strength, the relationship:

$$\sqrt{\left(\frac{f_c}{2}\right)^2 + \tau^2} = \frac{f_c}{2} + f_t \tag{96}$$

$$\tau = \sqrt{f_t^2 + f_c f_t} = f_c \sqrt{\left(\frac{f_t}{f_c}\right)^2 + \frac{f_t}{f_c}} \approx 0.33 f_c \tag{97}$$

Where $(f_c/f_t) = 0.1$, and the maximum failure occurs at the angle of:

$$\alpha = 45^o + (\beta/2) \tag{98}$$

Where β is determined by:

$$\tan\beta = 0.5 f_c / \tau \tag{99}$$

$$\tan\beta = 0.5 f_c / 0.33 f_c \tag{100}$$

Tan β = 1.52, and β = 56.6o, therefore α = 73.3o.

The cone slope angle is briefly discussed in [35, 36, 37]. The cone plug has curved profile starts from small initial angle, increases towards larger final angle. According to experimental result from [37], the average conical slope angle is α = 66o and α = 76o for normal strength concrete and for high strength concrete respectively. If we take average of above angles α = 45o and 73.3o which equals to 59.2o making difference of only 10% with the results of Dancygier [37].

The another important parameter is average shear stress applied to the cone surface, this helps in the development of motion equation during plugging stage [36]. The previous studies recommend Tresca criteria to estimate the average shear stress on the cone plug surface [36],

$$\tau_f = \frac{1}{\sqrt{3}} f_c \approx 0.58 f_c \tag{101}$$

In case of cone plug is considered as to be under compression by the projectile. From figure according Mohr's circle, the shear stress occurs at the angle of $\alpha = 59.2^o$ is:

$$\tau_f = \left(\sqrt{\left[\left(\frac{f_c}{2}\right)^2 + \tau^2\right]}\right)\cos(28.4^o) \approx 0.66 f_c \tag{102}$$

Which makes 13% difference than the above value, the important point should be always taken in consideration that the above analysis given in [2], and the analytical model in [36] are only for plain cement concrete not for reinforced cement concrete.

6.0 LIMITATION FOR RIGID PROJECTILE ASSUMPTION

Chen and Li suggested the study about limitation of rigid projectile in [43]. They suggested that the rigid projectile assumption can be identified by three regimes:

I. The rigid projectile penetration regime, which defines the valid range of the proposed framework.
II. The semi-hydrodynamic penetration regime, which is represented by the Alekseevskii-Tate model.
III. The hydrodynamic penetration regime, which treats projectile as fluid.

These three regimes appear with increasing impact velocity or with increasing impact function (I). The valid approximate range of the impact velocities for these three regimes are $10 < V_o < 1000$m/s, $1000 < V_o < 3000$m/s, and $V_o > 3000$m/s for rigid projectile regime, semi-hydrodynamic regime, and for hydrodynamic regime respectively. They recommend a method for the determination of transition point between above three regimes, by equation the penetration resistance σ_n to the dynamic strength of the projectile σ_y,

$$\sigma_n = \sigma_y$$

The upper limit for the rigid projectile regime (I_{c1}) can be obtained while the lower limit of the impact function for the semi-hydrodynamic regime (I_{c2}) is obtained through the alekseevskii-Tate model. The dynamic strength of the projectile is dependent of quasi-static strength of the projectile material σ_s through factor λ. Therefore $\sigma_y = \lambda\sigma_s$, where λ is dependent on the impact function. This empirical factor includes the influences of loading rate and hydrostatic pressure on the dynamic strength of the projectile material. There is two possible transitions were predicted.

If $I_{c1} < I_{c2}$, in this case transition exist gradual change:

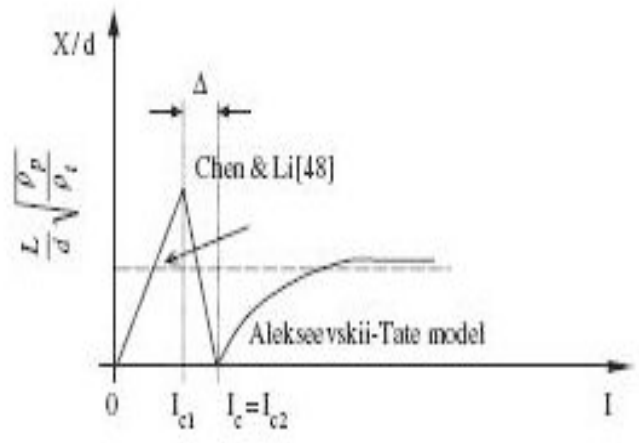

Fig. 17: Explains gradual from rigid projectile penetration to semi-hydrodynamic penetration [43]. In second possibility the transition may predicted suddenly:

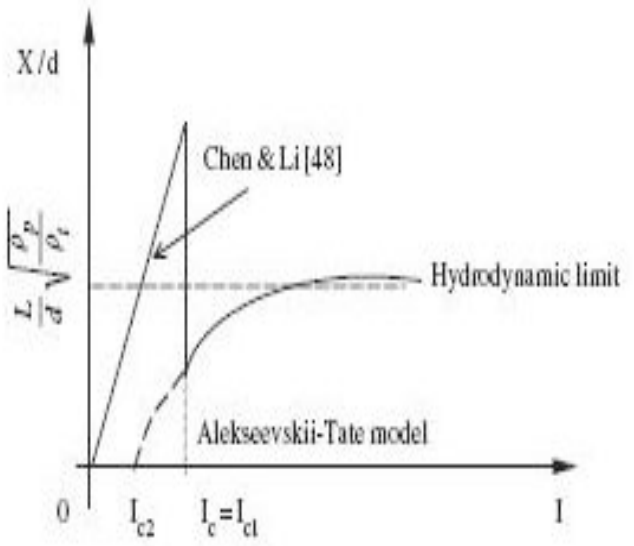

Fig. 18: Explains sudden transition from rigid projectile penetration to semi-hydrodynamic penetration [43].

Both situations were observed during experiments on metallic targets by Forrestal and Piekutowski [44], Piekutowaski et al. [45] and Hazell et al. [46]. The proposed method gave good predictions for the transition and transition point. Also Rosenberg and Dekel [47] adopted same method in their numerical study for prediction of transition between the rigid projectile regime and the eroding rod regime. The transition phenomenon was observed for metallic targets by using proposed method; however it also can be applied for concrete targets.

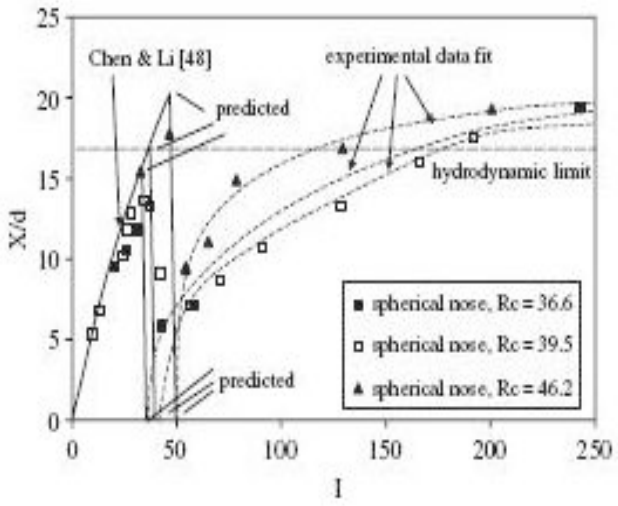

Fig. 19: Explains re-group of Forrestal and Piekutowski [44]'s penetration tests and the theoretical analysis [43].

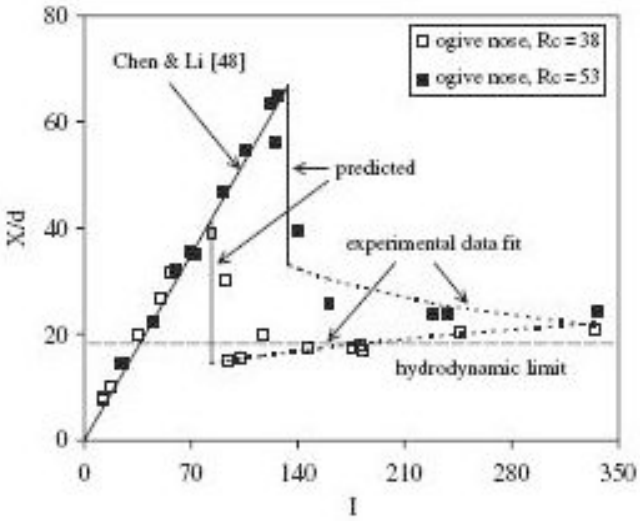

Fig. 20: Explains the re-group of Piekutowski et al. [45]'s penetration tests and the theoretical analysis [43].

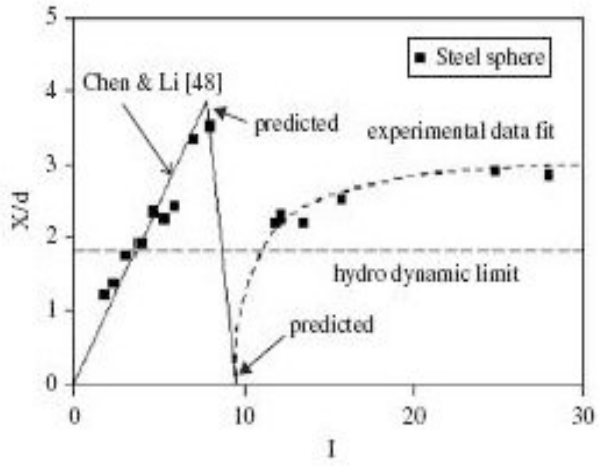

Fig. 21: Explains the re-group of Hazellet al. [46]'s penetration tests and the theoretical analysis [43].

4.0 CONCLUSION

In this paper the review have been done of the analytical studies on local impact effects on concrete and reinforced concrete structure against the impact of hard missile with and without the influence of dimensional analysis based on dominant non-dimensional parameters, various nose shape factors impacted at normal and certain inclined oblique angles. The paper comprises the analytical models and methods for predicting penetration, and perforation of concrete and reinforced concrete at normal and certain inclined oblique angles. For penetration the penetration resistance function has been summarized, for concrete and reinforced concrete at normal and at oblique angle. The multi – stage analytical models are also discussed for the perforation of concrete and reinforced concrete at normal and at oblique angle. The formation of a model for cone cracking also has been discussed including the cone cracking angle together with the limitations of hard missile assumptions.

5.0 REFERENCES

[1] Kennedy RP. A review of procedures for the analysis and design of concrete structures to resist missile impacteffects. Nucl. Eng. Des 1976;37:183–203.
[2] Li QM, Reid SR, Wen HM, Telford AR. Local impact effects of hard missiles on concrete targets. Int J Impact Eng 2005;32(1–4): 224–84.
[3] Warren TL, Poormon KL. Penetration of 6061-T6511 aluminum targets by ogive-nosed VAR 4340 steel projectiles at oblique angles: experiments and simulations. Int J Impact Eng 2001;25:993–1022.
[4] Allen WA, Mayfield EB, Morrison HL. Dynamics of a projectile penetrating sand. J Appl Phys 1957;28(3):370–6.
[5] Forrestal MJ, Tzou DY. A spherical cavity-expansion penetration model for concrete targets. Int J Solids Struct. 1997;34(31–32):4127–46.
[6] Forrestal MJ, Frew DJ, Hickerson JP, Rohwer TA. Penetration of concrete targets with deceleration-time measurements. Int J Impact Eng 2003;28:479–97.
[7] Wen HM. Penetration and perforation of thick FRP laminates. Compos Sci Technol 2001;61:1163–72.
[8] Wen HM. Predicting the penetration and perforation of targets struck by projectiles at normal incidence. Mech. Struct. Mach 2002;30(4):543–77.
[9] Bishop RF, Hill R, Mott NF. The theory of indentation and hardness tests. Proc Phys Soc 1945;57(Part 3):147–59.
[10] Hill R. A theory of earth movement near a deep underground explosion. Memo No. 21–48, Armament Research Establishment, Front Halstead, Kent, UK, 1948.
[11] Hopkins HG. Dynamic expansion of spherical cavities in metals. In: Sneddon IN, Hill R, editors. Progress in solid mechanics, vol. 1. Amsterdam, New York: North-Holland; 1960 Chapter 3.
[12] Goodier JN. On the mechanics of indentation and cratering in solid targets of strain-hardening metal by impact of hard and soft spheres. AIAA proceedings of the seventh symposium on hypervelocity impact III, 1965. p. 215–59.
[13] Forrestal MJ, Luk VK. Penetration into soil targets. Int J Impact Eng 1992;12:427–44.
[14] Forrestal MJ, Tzou DY, Askari E, Longcope DB. Penetration into ductile metal targets with rigid spherical-nose rods. Int J Impact Eng 1995;16:699–710.
[15] Li QM, Chen XW. Dimensionless formulae for penetration depth of concrete target impacted by a nondeformable projectile. Int J Impact Eng 2003;28(1):93–116.
[16] Forrestal MJ, Altman BS, Cargile JD, Hanchak SJ. An empirical equation for penetration depth of ogive-nose projectiles into concrete targets. Int J Impact Eng 1994;15(4):395–405.
[17] Forrestal MJ, Luk VK. Dynamic spherical cavity expansion in a compressible elastic–plastic solid. J Appl Mech ASME 1988;55:275–9.
[18] Luk VK, Forrestal MJ, Amos DE. Dynamics spherical cavity expansion of strain-hardening materials. ASME J Appl Mech 1991;58(1):1–6.
[19] Chen XW, Li QM. Deep penetration of a non-deformable projectile with different geometrical characteristics. Int J Impact Eng 2002;27:619–37.
[20] Xu Y, Keer LM, Luk VK. Elastic-cracked model for penetration into unreinforced concrete targets with ogival nose projectiles. Int J Solids Struct 1997;34(12):1479–91.
[21] Durban D, Masri R. Dynamic spherical cavity expansion in a pressure sensitive elastoplastic medium. Int J Solids Struct 2004;41:5697–716.
[22] Murff JD, Coyle HM. Low velocity penetration of Kaolin. ASCE J Soil Mech Found Div 1973;99(SM5):375–89.
[23] NDRC. Effects of impact and explosion. Summary Technical Report of Division 2, vol. 1, National Defence Research Committee, Washington, DC, 1946.
[24] Riera JD. Penetration, scabbing and perforation of concrete structure hit by solid missile. Nucl Eng Des 1989;115:121–31.
[25] Haldar A, Hamieh H. Local effect of solid missiles on concrete structures. ASCE J Struct Div. 1984;110(5):948–60.
[26] Heuze FE. Overview of projectile penetration into geological materials, with emphasis on rocks. Int J Rock Mech Min Sci Geomech Abstr 1990;27(1):1–14.
[27] Greighton DC. Non-normal penetration in soil and rock: user's guide for computer code PENCO2D. US Army Waterways Experiment Station, Vicksburg, Technical Report SL-82-7, 1982.
[28] Adley MD, Berger RP, Cargile JD, White HG, Greighton DC. Three dimensional projectile penetration into curvilinear geological/structural target. User's Guide for PENCRV3D, US Army Waterways Experiment Station, Instruction Report SL-97-1, Vicksbury, M.S., January 1997.
[29] Danielson KT, Adley MD. A meshless treatment of three-dimensional penetrator targets for parallel computation. Comput Mech 2000;25:267–73.

[30] Warren TL, Tabbara MR. Spherical cavity-expansion forcing function in PRONTO 3D for applications to penetration problems, SAND97-1174. Albuquerque, NM: Sandia National Laboratories; 1997.
[31] Warren TL, Tabbara MR. Simulations of the penetration of 6061-T6511 aluminum targets by spherical-nosed VAR 4340 steel projectiles. Int J Solids Struct 2000;37(3/2):4419–35.
[32] Warren TL. Simulations of the penetration of limestone targets by ogive-nose 4340 steel projectile. Int J Impact Eng 2002;16:699–710.
[33] Warren TL, Fossum AF, Frew DJ. Penetration into low-strength (23 MPa) concrete: target characterization and simulation. Int J Impact Eng 2004;30:477–503.
[34] Corbett GG, Reid SR, Johnson W. Impact loading of plates and shells by free-flying projectiles: a review. Int J Impact Eng 1996;18:141–230.
[35] Yankelevsky DZ. Local response of concrete slabs to low velocity missile impact. Int J Impact Eng 1997;19(4):331–43.
[36] Li QM, Tong DJ. Perforation thickness and ballistic performance of concrete target subjected to rigid projectile impact. ASCE J Eng Mech 2003;129(9):1083–91.
[37] Dancygier AN. Rear face damage of normal and high-strength concrete elements caused by hard projectile impact. ACI Struct J 1998;95:291–304.
[38] Hanchak SJ, Forrestal MJ, Young ER, Ehrgott JQ. Perforation of concrete slabs with 48 and 140MPa unconfined compressive strength. Int J Impact Eng 1992;12(1):1–7.
[39] Sliter GE. Assessment of empirical concrete impact formulas. ASCE J Struct Div 1980;106(ST5):1023–45.
[40] Barr P. Guidelines for the design and assessment of concrete structures subjected to impact. Report, UK Atomic Energy Authority, Safety and Reliability Directorate, HMSO, London, 1990.
[41] Li QM, Reid SR. Development of concrete impact models. Report to Magnox Electric Ltd., Report Reference:MAME/AM/0304/4500288589/JKL, Department of Mechanical, Aerospace and Civil Engineering, UMIST, 2004.
[42] BNFL. Reinforced concrete slab local damage assessment. R3 impact assessment procedure, Appendix H, vol. 3. Magnox Electric plc & Nuclear Electric Limited; 2003.
[43] Chen XW, Li QM. Transition from non-deformable projectile penetration to semi-hydrodynamic penetration. ASCE J Mech Eng 2004;130(1):123–7.
[44] Forrestal MJ, Piekutowski AJ. Penetration experiments with 6061-T6511 aluminum targets and spherical-nose steel projectiles at striking velocities between 0.5 and 3.0 km/s. Int J Impact Eng 2000;24:57–67.
[45] Piekutowski AJ, Forrestal MJ, Poormon KL, Warren TL. Penetration of 6061-T6511 aluminum targets by ogivenose steel projectiles with striking velocities between 0.5 and 3.0 km/s. Int J Impact Eng 1999;23:723–34.
[46] Hazell PJ, Fellows NA, Hetherington JG. A note on the behind armour effects from perforated alumina/aluminium targets. Int J Impact Eng 1998;22:589–95.
[47] Rosenberg Z, Dekel E. Numerical study of the transition from rigid to eroding-rod penetration. J Phys IV Fr 2003;110:681–6.
[48] Li QM, Reid SR, Ahmad-Zaidi AM. Critical impact energies for scabbing and perforation of concrete target. Nucl Eng Des 2006;236:1140–8.
[49] Chen XW, Fan SC, Li QM. Oblique and normal penetration/perforation of concrete target by rigid projectiles. Int J Impact Eng 2004;30(6):617–37.
[50] Dancygier AN, Yankelevsky DZ. High strength concrete response to hard projectile impact. Int J Impact Eng 1996;18(6):583–99.
[51] Recht RF, Ipson TW. Ballistic perforation dynamics. J Appl Mech -Trans ASME 1963;30:385–91.
[52] Ipson TW, Recht RF. Ballistic penetration resistance and its measurement. Exp Mech 1975;15:249–57.
[53] Forrestal MJ, Frew DJ, Hanchak SJ, Brar NS. Penetration of grout and concrete targets with ogive-nose steel projectiles. Int J Impact Eng 1996;18(5):465–76.
[54] Li QM, Chen XW. Penetration into concrete targets by a hard projectile. Structures under shock and impact VII. In: JonesN, Brebbia CA, Rajendran AM, editors. Seventh International Conference on Structures under Shock and Impact (SUSI/7). May 27–29, Montreal, Southampton: WIT Press; 2002. p. 91–100.
[55] Buzaud E, Laurensou R, Darrigade A, Belouet P, Lissayou C. Hard target defeat: an analysis of reinforced concrete perforation process. The 9th International Symposium on Interaction of the Effects of Munitions with Structures, Berlin, Germany; 3–7 May, 1999, pp. 283–290.
[56] Dancygier AN. Effect of reinforcement ratio on the resistance of reinforced concrete to hard projectile impact. Nucl Eng Des, 1997;172:233–45.
[57] Wang, Z.L., Y.C. Li, R.F. Shen and J.G. Wang, 2007. Numerical study on craters and penetration of concrete slab by ogive nose steel projectile. Comput. Geotech., 36: 1-9.